Staircase-Free Finite-Difference Time-Domain Formulation for General Materials in Complex Geometries

K. H. Dridi, Jan S. Hesthaven, and Adi Ditkowski

***Abstract*—A stable Cartesian grid staircase-free finite-difference time-domain formulation for arbitrary material distributions in general geometries is introduced. It is shown that the method exhibits higher accuracy than the classical Yee scheme for complex geometries since the computational representation of physical structures is not of a staircased nature. Furthermore, electromagnetic boundary conditions are correctly enforced. The method significantly reduces simulation times as fewer points per wavelength are needed to accurately resolve the wave and the geometry. Both perfect electric conductors and dielectric structures have been investigated. Numerical results are presented and discussed.**

***Index Terms*—Computational models in electromagnetics and optics, finite-difference time-domain methods, numerical solution of partial differential equations, staircase, time-domain solution of Maxwell's equations.**

I. Introduction

THE need for higher capacity and higher speed telecommunication and computing systems requires the ongoing miniaturization and integration of optical waveguide technology and components of diverse optical electromagnetic properties such as diffractive gratings, antennas, photonic crystal structures, etc. This puts high requirements on modeling and design tools, which should offer modest solution times and good accuracy in space and time for general large scale structures of finite or infinite dimensions. Furthermore, the complex subwavelength geometry and multidimensional material composition of physical structures often prohibits an exact analytical solution and deceives the intuitive understanding of their physics. Therefore, it is often desirable to solve Maxwell's vectorial curl equations with as few approximations as possible to get a realistic insight. A number of such vectorial numerical methods as the finite-difference time-domain (FDTD) method [1]–[9] and the spectral method [10]–[15] have succesfully been applied to solve Maxwell's equations for a wide range of problems. The original FDTD method has the advantage of being relatively simple in its formulation and its definition of the geometry (grid-layout) because no complicated and time-consuming mesh generation is needed. The spatial second-order accurate FDTD scheme is still the most popular method as higher order methods use field information further away to evaluate spatial derivatives at each point, making them a bit more complicated for problems in complex geometries. However, the FDTD approach based on the classical Yee scheme [1] with quadratic cell mapping in space gives the modeled structures a "staircase nature" and requires many points per wavelength to efficiently resolve the geometry and the minimal material wavelength. Furthermore, the classical FDTD approach is ill-suited for arbitrary geometries with multiple materials as the electromagnetic boundary conditions are not automatically nor exactly imposed and satisfied at these boundaries [16]–[18], which presents an additional source of local spatial errors besides the the numerical dispersion due to the spatial and temporal second-order nature of the scheme. The larger the computational domain and the more complex the material distributions are, the more the noise accumulates in the numerical solution. These errors grow at least linearly in time for a second-order scheme. Some reports on the issues of the staircasing problem in connection with the FDTD method can be found in the literature [16], [17]. Some effects of staircasing have been studied for simple geometries; however, a general remedy for more complex problems still needs to be found, especially because general geometries rarely have contour lines that fit on the discrete gridpoints of the chosen mesh in a particular coordinate system, making the exact application of field boundary conditions at material interfaces impossible without the averaging of material parameters. The boundary conditions are not imposed exactly by this averaging in regions that are not geometrically clearly resolved near material interfaces.

In order to enforce the boundary conditions, eliminate the effects of staircasing, and reduce the required number of points per wavelength, a stable second-order accurate FDTD formulation is presented. The numerical scheme can be adapted and applied to dielectrics as well as perfect electric conductors (PECs) of general geometry.

Section II is concerned with the basic principles of the method in one-dimensional (1-D) space. It is described how the new FDTD method supports the correct application of electromagnetic boundary conditions, and numerical experiments are presented for a 1-D PEC cavity filled with two dielectrics. The numerical accuracy of the Yee scheme and the new formulation is compared. In Section III, two-dimensional (2-D) models are described and numerical results are presented for two case studies. The first test case is a PEC resonator of cylindrical shape, whereas the second one concerns a dielectric cylinder

Manuscript received June 30, 1999; revised August 10, 2000.

K. H. Dridi was with the Research Center COM, Technical University of Denmark, DK-2800 Lyngby, Denmark. He is now with the Optics and Fluid Dynamics Department, OFD-129, Risø National Laboratory, DK-4000 Roskilde, Denmark.

J. S. Hesthaven and A. Ditkowski are with the Division of Applied Mathematics, Brown University, Providence, RI 02912 USA.

Publisher Item Identifier S 0018-926X(01)05256-5.

illuminated by a plane wave. Section IV contains a few concluding remarks.

II. The Fundamentals

Classical electromagnetic behavior is governed by the four macroscopic Maxwell equations and the constitutive relations. We restrict the analysis to nonmagnetic, charge-free, linear, and locally isotropic media. However, these assumptions are not restrictions imposed by the method. We have

$$\nabla \cdot [n^2 \mathbf{E}] = 0, \quad \nabla \cdot \mathbf{H} = 0 \tag{1}$$

$$\nabla \times \mathbf{E} = -\frac{\partial \mathbf{H}}{\partial t}, \quad \nabla \times \mathbf{H} = n^2 \frac{\partial \mathbf{E}}{\partial t} \tag{2}$$

where $\mathbf{E}$ and $\mathbf{H}$ are the macroscopic electric (normalized with the free space intrinsic impedance Z_0) and magnetic fields, respectively, and n is the index of refraction of the medium. All spatial coordinates have been normalized with the free-space wavelength λ, while t is the time variable normalized with the temporal field oscillation period λ/c (c is the speed of light in vacuum). The electromagnetic solution is determined by the following material-dependent general boundary conditions [19] (see Fig. 1):

$$\mathbf{0} = \hat{\mathbf{n}}_1 \times \mathbf{E}_1 + \hat{\mathbf{n}}_2 \times \mathbf{E}_2 \tag{3}$$

$$-\mathbf{J}_e^s = \hat{\mathbf{n}}_1 \times \mathbf{H}_1 + \hat{\mathbf{n}}_2 \times \mathbf{H}_2 \tag{4}$$

$$-\frac{\rho_e^s}{Z_0} = \hat{\mathbf{n}}_1 \cdot (\epsilon_1 \mathbf{E}_1) + \hat{\mathbf{n}}_2 \cdot (\epsilon_2 \mathbf{E}_2) \tag{5}$$

$$0 = \hat{\mathbf{n}}_1 \cdot (\mathbf{H}_1) + \hat{\mathbf{n}}_2 \cdot (\mathbf{H}_2) \tag{6}$$

where

- $\mathbf{J}_e^s$ electric surface current density;
- ρ_e^s electric surface charge density;
- $\hat{\mathbf{n}}_1$ and $\hat{\mathbf{n}}_2$ surface normal vectors;
- ϵ_i where $i = 1, 2$, is the permittivity.

To introduce the numerical scheme, we consider the following partial differential equations in a 1-D Cartesian coordinate system with multiple materials (see Fig. 2):

$$\left[\frac{\partial E_y}{\partial t}, \frac{\partial H_z}{\partial t}\right] = \left[\frac{1}{n^2(x)} \frac{\partial H_z}{\partial x}, \frac{\partial E_y}{\partial x}\right]. \tag{7}$$

For simplicity, it is assumed that each area is homogeneous with respect to electromagnetic properties of the medium, in this case the index of refraction. We define our computational domain to include the physical space, $[x_1; x_N]$. The gridline contains N segments where $h_x = (x_N - x_1)/(N-1)$. In the interior of the regions we apply the staggered scheme such that the electric and magnetic field points alternate, separated by $0.5h_x$, as second-order staggered schemes for Maxwell's equations are more attractive in terms of accuracy and stability [20]. Each region has two outer points within its area, before or on the material boundaries on its left and right side. These outer points can either be "electric or magnetic field points." Each area is then assigned two values, γ_l and γ_r, where $\gamma_l h_x$ is the distance from the left boundary to the first point in the area and $\gamma_r h_x$ the distance from the right boundary to the last point in the area. Obviously, γ values are to be found within $[0; 0.5]$. It is possible to find finite difference weights to evaluate spatial derivatives

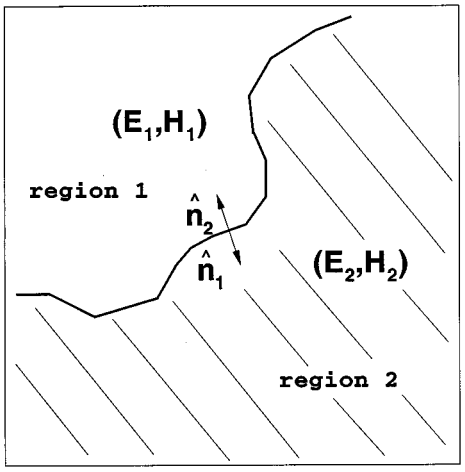

Fig. 1. Boundary between regions 1 and 2 with surface normal vectors.

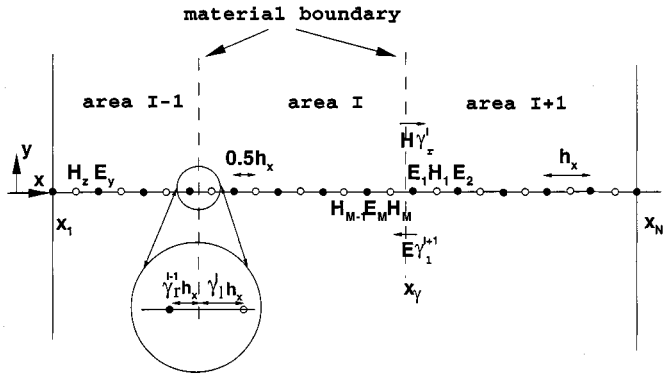

Fig. 2. Mapping in 1-D space composed of several areas (subspaces) with different refractive indexes. A staggered grid is defined in a Cartesian coordinate system.

of any order m, approximated to any level of accuracy at any point x' with the help of an algorithm based on Lagrange interpolation polynomials [21]. The point x' need not be a grid point. We shall exploit this to make interpolations and extrapolations needed to get rid of the staircasing problem and apply the correct electromagnetic boundary conditions.

A. Boundary Between Two Dielectrics

In the case of a boundary between two dielectrics at x_γ (see Fig. 2), the boundary conditions state that the tangential electric and magnetic fields are continuous at material boundaries [19]. We consider the spatial second-order accurate case. In this case all spatial derivatives at inner points in each area are computed as in the Yee scheme with two symmetrically surrounding points. Spatial derivatives at the outer points are evaluated along the gridlines using the following approximations of first-order accuracy where we apply the boundary conditions. We describe the case where area I "ends with a magnetic field point H_M" and area $I+1$ "starts with an electric field point E_1." The reversed situation is treated similarly. At the field position of E_1 we assume

$$\frac{\partial H}{\partial x} \cong \frac{\partial H}{\partial x}\Big|_{x_\gamma} \cong \frac{H_1 - H_{\gamma_r^I}}{(\frac{1}{2} + \gamma_l^{I+1}) h_x} \tag{8}$$

where $H_{\gamma_r^I}$ is the tangential magnetic field value that is extrapolated from within area "I" to the material interface (at x_γ) as

$$H_{\gamma_r^I} \cong \frac{H_M - H_{M-1}}{h_x}(\gamma_r^I h_x) + H_M \tag{9}$$

which is a linear extrapolation. Similarly, at the field position of H_M we have

$$\frac{\partial E}{\partial x} \cong \frac{\partial E}{\partial x}|_{x_\gamma} \cong \frac{E_{\gamma_l^{I+1}} - E_M}{(\frac{1}{2} + \gamma_r^I)h_x} \tag{10}$$

where $E_{\gamma_l^{I+1}}$ is the tangential electric field value that is extrapolated from within area "I + 1" to the material interface (at x_γ) as

$$E_{\gamma_l^{I+1}} \cong \frac{E_2 - E_1}{h_x}(-\gamma_l^{I+1} h_x) + E_1 \tag{11}$$

which is a linear extrapolation. This leads to (12)–(15). In evaluating the field derivatives at outer points in (12) and (13), we apply the electromagnetic boundary conditions such that field information is communicated between the areas at the interface, with area I getting tangential electric field information $E_{\gamma_l^{I+1}}$ from area $I+1$, while area $I+1$ gets tangential magnetic field information $H_{\gamma_r^I}$ from area I as

$$\frac{\partial E_1}{\partial t} \cong \frac{1}{n_{I+1}^2}\frac{2}{1+2\gamma_l^{I+1}}\frac{H_1 - H_{\gamma_r^I}}{h_x} \tag{12}$$

$$\frac{\partial H_M}{\partial t} \cong \frac{2}{1+2\gamma_r^I}\frac{E_{\gamma_l^{I+1}} - E_M}{h_x} \tag{13}$$

$$H_{\gamma_r^I} \cong (1+\gamma_r^I)H_M - \gamma_r^I H_{M-1} \tag{14}$$

$$E_{\gamma_l^{I+1}} \cong (1+\gamma_l^{I+1})E_1 - \gamma_l^{I+1}E_2. \tag{15}$$

Here (14) and (15) represent one-sided extrapolations that are subsequently used in (12) and (13) to update E_1 and H_M. Looking at the denominators in (12) and (13), we notice that as γ values tend to 0 or 0.5 the fractions remain finite (an average refractive index is used in rare cases where gridpoints coincide with the material boundary), indicating the well-posedness and stability of this scheme. A similar scheme is used in the case where the first (last) point of an area is a magnetic(electric) field point.

B. Boundary Between a Dielectric and a Perfect Electric Conductor

In the case of a boundary between a dielectric and a perfect electric conductor (PEC) at x_γ (see Fig. 2), the boundary conditions express that the tangential electric field is zero [19]. The spatial derivatives at these outer points are evaluated using the following approximations of first-order accuracy where we apply the boundary conditions. In a situation where area $I+1$ is filled with a PEC material and area I contains a dielectric, all fields in area $I+1$ are zero, and following the exact same approximations as in the previous case with a material interface between two dielectrics, but where tangential electric fields are zero, we have the following approximation:

$$\frac{\partial H_M}{\partial t} \cong \frac{2}{1+2\gamma_r^I}\frac{E_{\gamma_l^{I+1}} - E_M}{h_x} \tag{16}$$

$$E_{\gamma_l^{I+1}} = 0. \tag{17}$$

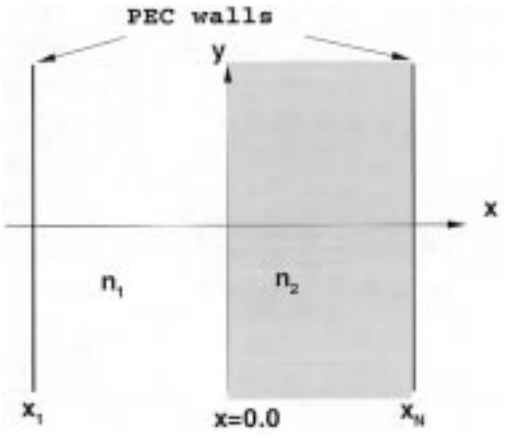

Fig. 3. PEC cavity filled with two dielectrics.

In the next situation, where area I is filled with a PEC material and area $I+1$ contains a dielectric, all fields in area I are zero and we apply the following approximation:

$$\frac{\partial E_1}{\partial t} \cong \frac{1}{n_{I+1}^2}\frac{\gamma_l^{I+1}}{1+\gamma_l^{I+1}}\frac{H_2 - H_1}{h_x}. \tag{18}$$

C. PEC Cavity Filled with Two Dielectrics

Fig. 3 shows a PEC cavity with two dielectric materials of refractive indexes n_1 and n_2, respectively. The PEC walls are located at $x = x_1$ and $x = x_N$, and the dielectric material boundary is at $x = 0.0$ in a geometry that is invariant in the y- and z-dimension. A staggered grid where electric field points are located at $x = x_1$ and $x = x_N$ is used to solve the set of (7), where $n(x)$ is the refractive index of the medium. The boundary conditions for the fields express that the tangential electric field is zero at the PEC walls, while all tangential field components are continuous at $x = 0.0$. When $x_1 = -1.0$ and $x_N = 1.0$, the analytic solution to this problem is

$$E_{yi} = (A_i \exp(jn_i\omega x) - B_i \exp(-jn_i\omega x))\exp(j\omega t) \tag{19}$$

$$H_{zi} = n_i(A_i \exp(jn_i\omega x) + B_i \exp(-jn_i\omega x))\exp(j\omega t) \tag{20}$$

where $i = 1, 2$ and $j = \sqrt{-1}$ and

$$A_1 = \frac{n_2 \cos(n_2\omega)}{n_1 \cos(n_1\omega)} \tag{21}$$

$$A_2 = \exp(-j\omega(n_1 + n_2)) \tag{22}$$

$$B_1 = \exp(-j2n_1\omega)A_1 \tag{23}$$

$$B_2 = \exp(j2n_2\omega)A_2. \tag{24}$$

To determine ω when the refractive indexes are defined, we solve the following transcendental equation numerically:

$$-n_2 \tan(n_1\omega) = n_1 \tan(n_2\omega). \tag{25}$$

We take $n_1 = 1.0$, $n_2 = 1.5$ and $\omega = 5.072\,181\,161\,825\,156\,9$ and define the $L_2(t)$ error as

$$L_2(t) = \sqrt{\frac{\sum_{i=1}^{N}(H_{zi}^{\text{EXACT}} - H_{zi}^{\text{NUM}})^2}{N}} \tag{26}$$

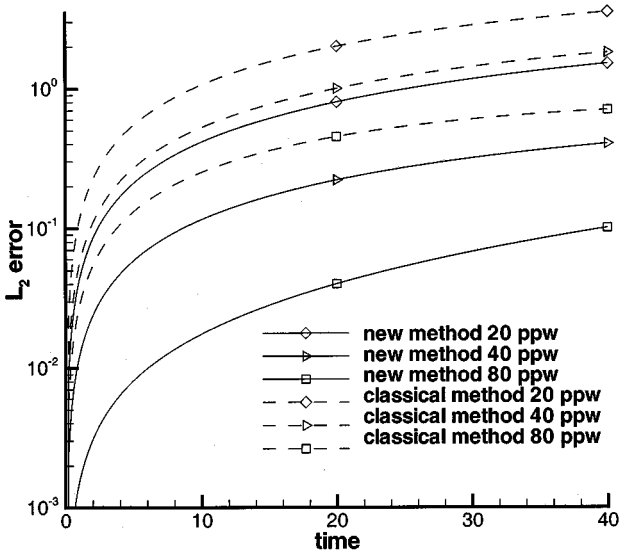

Fig. 4. L_2 error as a function of time for the new and the classical FDTD methods for the PEC cavity filled with two dielectrics for resolutions of 20, 40, and 80 ppw.

to estimate the numerical errors for the Yee scheme and the new technique. The fields experience a jump at the material interface and different velocities of propagation together with different material wavelengths in each homogeneous area, in each of which the solution is smooth. In the classical FDTD method based on the Yee scheme, the fields are approximated by a second-order polynomial, but the material interface does not necessarily coincide with a grid point for different choices of resolution, and the spatial derivatives are taken across the material interface around which the material parameters are averaged. In fact, the poorly resolved representation of general geometric structures in the discretized computer model cannot be avoided once a fixed coordinate system is chosen, unless a multidomain approach is considered. In the present new method, the same grid layout as the one for the classical FDTD is used, but the intersection of the material interface (object contour) with the gridline is detected, and two areas of different refractive indexes are defined together with the line segment characteristics according to the approach discussed previously in this section. For each area, two γ values are computed once the grid layout and resolution have been chosen. The only main difference between the classical scheme and the new method is in the technique of treating spatial derivatives at outer points of each area filled with a homogeneous dielectric. In this manner, the material interface is represented correctly, and field boundary conditions can be applied correctly. Fig. 4 shows the L_2 error as a function of time for the classical FDTD (Yee scheme) and the new second-order schemes, respectively, for the PEC cavity filled with two dielectrics with resolutions of 20, 40, and 80 points per wavelength (ppw). It is noticeable that the Yee scheme is not of spatial second-order accuracy but rather only of first-order accuracy in this case where two obejcts with different materials are present. This is due to the fact that the boundary conditions are not properly satisfied, that the material interface is not represented correctly, and that spatial derivatives are taken across material boundaries. As anticipated, the new second-order FDTD formulation really shows spatial second-order accuracy, i.e., the error behaves as $O(h_x^2)$. Errors at a given time decrease by a factor of four when the number of points per wavelength is multiplied by two. Furthermore, the new formulation is much more accurate because of its correct implementation of the boundary conditions. The order of accuracy of a numerical scheme, or the convergence of the solution, can be recovered or at least enhanced by improving the representation of physical structures and by the correct application of boundary conditions at better resolved interfaces. It is clear that for a fixed accuracy, this improvement in convergence, even for such a simple 1-D problem, enables the use of fewer ppw with the new method in order to solve a computaional problem, thereby obtaining simulation times that are quite faster, as the time step is directly proportional to the discrete spatial step.

Regarding the numerical dispersion, it is known that the use of second-order schemes requires more points per wavelength to reduce errors in phase velocities. An alternative to spatial second-order schemes can be found in fourth-order FDTD or higher order spectral methods. A staircase free fourth-order FDTD scheme has been developed for 1-D problems with complex geometries [8], but to our knowledge no unconditionally stable 2-D schemes have been designed yet. In higher order schemes, fields are approximated by higher order polynomials. Thus, more terms of the Taylor expansion are included, thereby reducing the numerical dispersion, as the local computation of fields is based on global field information at all grid points. The numerical dispersion can be reduced to a minimum with spectral methods [10]–[15], and complex geometries can be modeled with the use of a multidomain approximation, in which staircasing is avoided, boundary conditions can be set correctly at the sub-domain boundaries, and where characteristic variables and proper mapping of geometries from real physical coordinates to local curvilinear coordinate systems can be applied.

III. Numerical Models in 2-D Space

In Fig. 5 is illustrated a model representation of physical structures in the computational window. The top figure shows the physical structure. The second one shows the structure represented with a discrete staircase approximation typical for the Yee method where each cell is assigned one refractive index value (the structure is represented by the set of cells that are crossed). The bottom figure shows the physical structure represented accurately without staircasing where intersections of the contour of the object and the gridlines have been marked. The physical representation with the staircased profile clearly needs a much higher resolution to be an acceptable model for the physical geometry and it requires more data storage and longer simulation times. Furthermore, the exact application of general material boundary conditions is not possible, and the taking of spatial derivatives across dielectric material boundaries is a source of errors in computational simulations for general geometrical shapes.

For PEC structures, a recent study showed the degradation of numerical accuracy due to the staircasing effect [18] in a 2-D

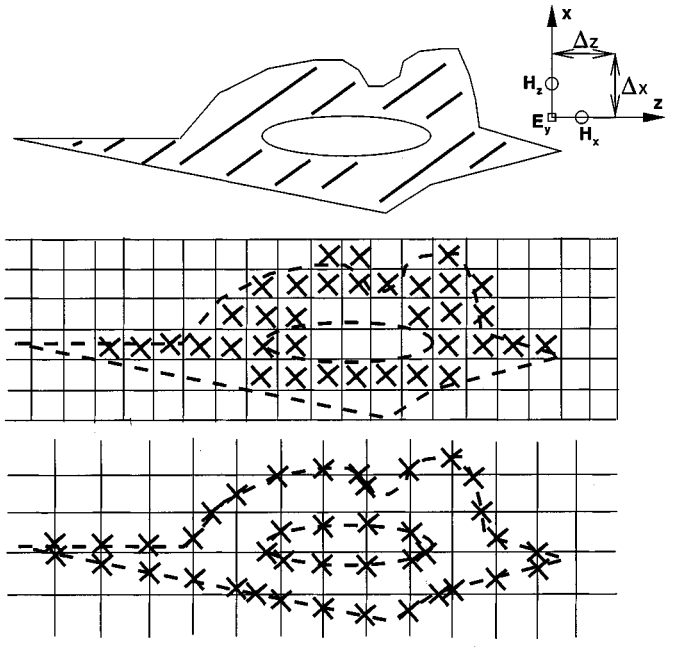

Fig. 5. Model representations of physical structures in the computational window. The top figure shows the physical structure. The middle figure shows the structure represented with a staircase approximation typical of the Yee method. The bottom figure shows the physical structure represented accurately without staircasing. The physical representation with the staircased profile needs a higher resolution to be an acceptable model for the physical geometry. A Cartesian coordinate system is defined with electromagnetic field components. Δx and Δz are the discrete spatial steps.

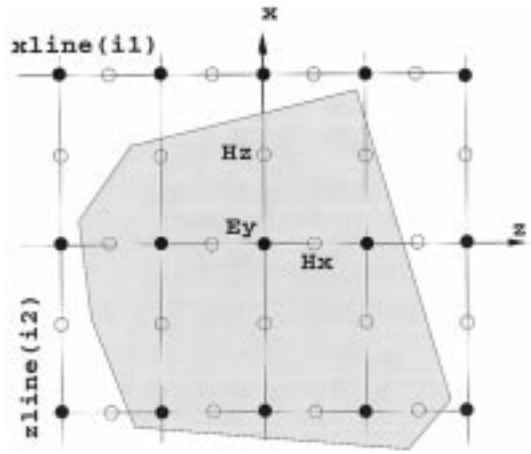

Fig. 6. Two-dimensional mesh for the new FDTD method in a Cartesian coordinate system.

problem. If we use the mesh configuration depicted in Fig. 6 with the three field components E_y, H_x, and H_z, we can apply the 1-D technique presented in the previous section to each gridline one by one, dimension by dimension, where E_y is the field component used for connectivity, i.e., for passing field information from one line in one dimension to another line in the second dimension. In Fig. 6 a gridline that is parallel to $\hat{\mathbf{z}}(\hat{\mathbf{x}})$ is denoted by x(z)-line, with i_1 and i_2 being indexes. If we wish to solve the TE equations on the form

$$n^2\frac{\partial E_y}{\partial t} = \frac{\partial H_x}{\partial z} - \frac{\partial H_z}{\partial x} \tag{27}$$

$$\frac{\partial H_x}{\partial t} = \frac{\partial E_y}{\partial z} \tag{28}$$

$$\frac{\partial H_z}{\partial t} = -\frac{\partial E_y}{\partial x} \tag{29}$$

numerically, we need to update $[n^2\partial E_y/\partial t, \partial H_x/\partial t]$ with $[\partial H_x/\partial z, \partial E_y/\partial z]$ along each xline(i_1) for all i_1, then update $[n^2\partial E_y/\partial t, \partial H_z/\partial t]$ with $[-\partial H_z/\partial x, -\partial E_y/\partial x]$ along each zline(i_2) for all i_2, at each time step, where special attention must be given to outer points of each area (subspace) along each gridline. A gridline must have some data associated with it, i.e., its number of areas, and for each of these, two γ values, a logical variable indicating whether the last point in an area before the material boundary is an electric or a magnetic field point and the global index of this last point. A preprocessing operation should be done to determine these records for each gridline, where intersections of object contours and gridlines must be detected. Any one area must contain at least two electric and two magnetic field points. The new technique follows the principle of the method of lines and permits a multidomain approach in a Cartesian grid. With this new formulation the staircasing error is eliminated and boundary conditions are satisfied and implemented correctly. The only errors introduced are γ–dependent extrapolation errors at material boundaries. When material distributions are arbitrary and large objects or fine subwavelength structures are under study, the comparison of error levels for the classical Yee scheme and the new technique shows significant improvement in favor of the newly formulated method. For a fixed accuracy, the new FDTD formulation will need many fewer points per wavelength than the Yee scheme to simulate the electrodynamics.

We use fourth-order accurate Runge–Kutta methods for the time derivatives [22]. The stability criterion that we apply for 2-D time-domain problems is [23]

$$\Delta t \leq \frac{5\sqrt{8}\min(\Delta x, \Delta z)}{13c} \tag{30}$$

where Δt is the discrete time step, c is the speed of light in vacuum, and where we choose the smallest spatial step. For a more detailed mathematical analysis on the properties of the method see [23] in which the stability of the scheme is proven. It is worth noticing that the maximal allowed time step for the new method is 20/13 times larger than that of the classical Yee scheme. The spatial step is chosen such that the geometries and the minimal material wavelength are resolved to an acceptable degree of accuracy.

For continuous-wave illumination in total field/scattered field formulations, the incident field must be added or subtracted at a few discrete points in the computational domain, at each intermediate step in the Runge–Kutta iteration for each time step. At these discrete points, the incident field that is added or subtracted must be computed with the same Runge–Kutta algorithm to get incident field data that are synchronized at the time corresponding to each step of the Runge–Kutta iteration.

In the following analysis we use a total-field/scattered-field formulation with a perfectly matched layer [15] terminated with a PEC wall for the new formulation and the FDTD model based on the Yee scheme developed in [5].

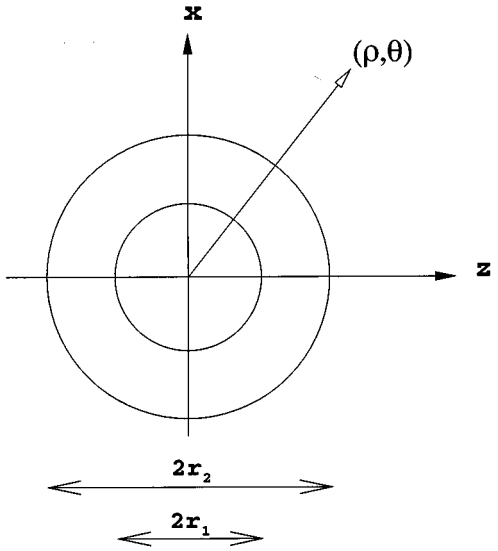

Fig. 7. Perfect electric conductor (PEC) resonator of cylindrical shape.

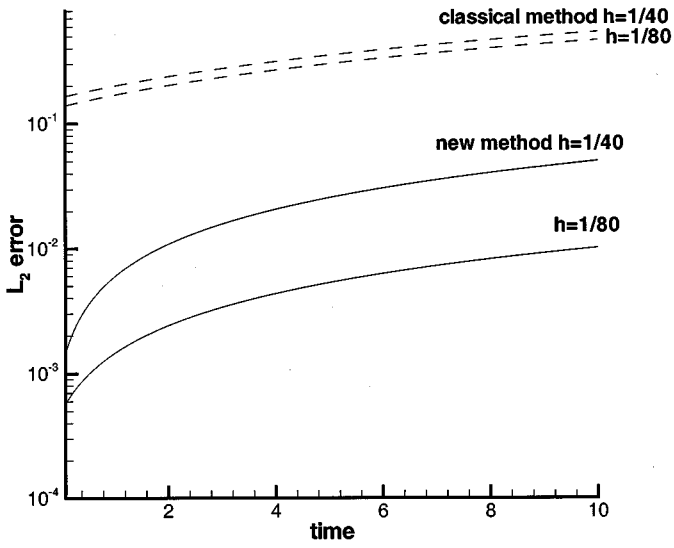

Fig. 8. L_2 error for the new and the classical FDTD schemes for the (PEC) resonator of cylindrical shape where h is the spatial step.

A. A PEC Resonator of Cylindrical Shape

The new FDTD formulation has been tested in a case study where a cylindrical perfect electric conducting resonator is defined in the (z, x) plane as shown in Fig. 7. It is assumed that the electromagnetic field is composed of transverse electric (TE) waves. The structure is invariant in the y-direction, and the electromagnetic field is indepedent of the y-coordinate. The free space wavelength-normalized radii of the two cylinders are $r_1 = 1/6$ and $r_2 = 1/2$. For $\rho < r_1$ and $\rho > r_2$, magnetic and electric fields are assumed to be zero. For $r_1 < \rho < r_2$, the space is filled with air, and the fields behave according to Maxwell's curl laws, while at $\rho = r_1$ and $\rho = r_2$ metallic PEC boundary conditions are imposed. The analytical solution for this simple problem is rather trivial [8]. The application of the new method in this case is done by defining a square computational domain that includes the outer cylinder. The origin of the Cartesian grid is then placed at the center, and for each gridline the intersections with the object contours are detected, and its number of areas (line segments), the γ values, etc., are recorded. In this particular case, areas on a gridline are defined as the line segments along which the fields are either existant ($\rho > r_1$ and $\rho < r_2$) or nonexistant ($\rho < r_1$ and $\rho > r_2$). In the latter case, no computations are needed along the corresponding line segments. The new method is then applied as explained for 2-D problems with the 1-D scheme introduced in Section II, in which there is an interface between a dielectric (air in this case) and a PEC wall (the cylinder contours). A preprocessing routine determines all the necessary line-segment records.

Fig. 8 shows the L_2 error of the electric field component as a function of time for the new and the classical FDTD schemes for different resolutions, where h denotes the spatial step. It is apparent that the new formulation exhibits errors that are more than one order of magnitude smaller than the Yee scheme. Note that as the resolution is increased the error decreases significantly for the new FDTD scheme, where spatial second-order convergence is apparent; whereas this is not the case for the Yee scheme, which approaches an error below that of first order accuracy.

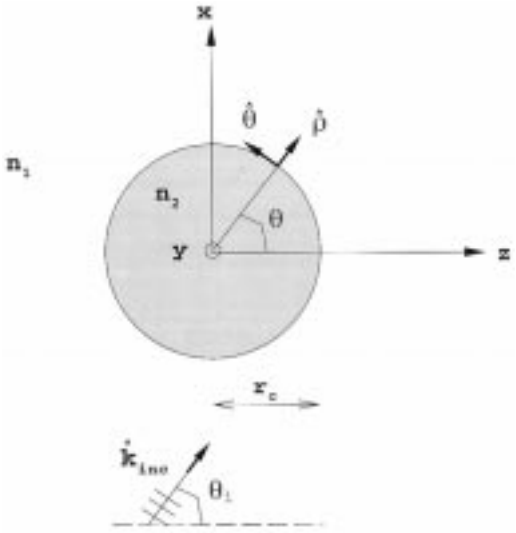

Fig. 9. Plane wave incidence on a dielectric cylinder.

B. Plane Wave Incidence on a Dielectric Cylinder

Fig. 9 shows a plane wave propagating in a medium with refractive index $n_1 = 1$ toward a dielectric cylinder with refractive index $n_2 = 1.5$ and radius r_c. The angle of incidence is θ_i. We assume that the electromagnetic field and the geometry are invariant in the y-direction. We have

$$\frac{\partial H_\rho}{\partial t} = -\frac{1}{\rho}\frac{\partial E_y}{\partial \theta} \tag{31}$$

$$\frac{\partial H_\theta}{\partial t} = \frac{\partial E_y}{\partial \rho} \tag{32}$$

$$\frac{\partial E_y}{\partial t} = \frac{1}{n^2(\rho)}\left[\frac{H_\theta}{\rho} + \frac{\partial H_\theta}{\partial \rho} - \frac{1}{\rho}\frac{\partial H_\rho}{\partial \theta}\right] \tag{33}$$

where the electric field has been normalized with the intrinsic impedance of free space, $\rho = \sqrt{z^2 + x^2}$, θ is the angle defined in Fig. 9, t is the time variable normalized with the temporal

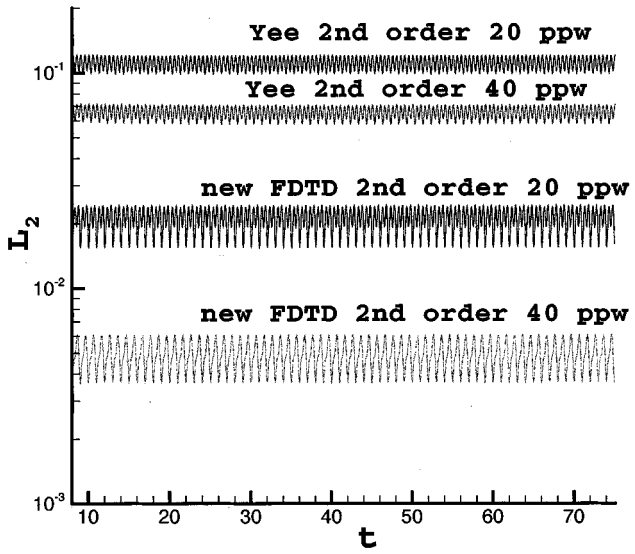

Fig. 10. L_2 error as a function of time for the second-order Yee scheme and the new FDTD formulation.

oscillation period λ/c, and all coordinates have been normalized with the free space wavelength, while $n(\rho)$ is the refractive index. Again, the analytical time harmonic (E_y, H_x, H_z) solution for this simple problem is rather trivial [8]. The application of the new method to this problem is similar to the case of the PEC cylindrical resonator, except that the definition of areas (line segments) is now made on the basis of the dielectric material, and that the finite difference schemes used on each gridline are the 1-D schemes presented in Section II for a material interface between two dielectrics.

Fig. 10 shows the L_2 error of the H_z component as a function of time for the Yee scheme and the new FDTD formulation of spatial second-order accuracy for different resolutions, i.e., 20 and 40 ppw. The plots start at $t = 8$ where all fields have reached steady state and end at $t \sim 75$, but the L_2 levels have been monitored until $t = 565$. Fig. 10 clearly shows that the Yee method, which is a spatial second-order accurate method in a homogeneous medium, does not show second-order convergence when applied to structures with more general geometries and different materials. This is partly due to the fact that it does not allow the electromagnetic boundary conditions to be applied correctly, and partly due to the staircasing problem. The error levels of the new second-order accurate FDTD method are approximately five times lower for 20 ppw and more than ten times lower for 40 ppw than the ones for the Yee scheme. As the resolution increases the new formulation increases its accuracy relative to the Yee scheme. The maximal allowable time step used with the new method is 20/13 times larger than that of the Yee scheme, and in order to achieve the accuracy of the new method for 20 ppw, the Yee scheme must use 85 ppw. Several performance tests have been done to compare the simulation times, and it is concluded that the new method is about 2.5 times faster for the actual problem on a 600-MHz Pentium PC. The new technique offers a fairly simple way of improving some of the deficiencies of the classical FDTD method for 2-D problems.

It is clear that as many more objects of general geometries (that do not necessarily have contour lines that follow the gridlines, or fit on the grid points) and different materials are introduced into the computaional domain, numerical errors grow even more due to the staircasing effect and the lack of application of material boundary conditions in the classical FDTD method. These errors have to be added to the numerical dispersion inherent in low-order schemes. This must be expected to be even more pronounced for 2-D problems with TM polarized fields, and in 3-D models with general polarizations with general material boundaries with surface electric or magnetic sources.

IV. Conclusion

A stable multispace staircase-free FDTD method of spatial second-order accuracy has been developed. Contrary to the classical Yee scheme, it allows the correct application of electromagnetic boundary conditions. Moreover, it does not represent the physical structure using a staircase approximation, but takes into account the exact geometry, and thus significantly reduces the required number of points per wavelength to accurately resolve the wave and the geometry, therefore allowing simulation times that are about two to three times faster than that of classical methods. Numerical experiments have shown that the improvement of the computational representation of geometries, avoiding staircasing and enabling the correct application of boundary conditions, can improve the convergence of the numerical methods significantly, and allows the use of lower resolutions. The new formulation is applicable to general geometries with arbitrary distributions of material in Cartesian coordinate systems. Numerical simulations show that it exhibits error levels that are orders of magnitude lower than what was achieved up until now with the classical Yee scheme for very general physical problems involving dielectrics as well as perfect electric conductors. The test cases in this paper have included a 1-D PEC cavity filled with two dielectrics, plane wave incidence on a dielectric cylinder, and a PEC resonator of cylindrical shape in 2-D space, but the new technique has also been applied to study the physics of complex subwavelength diffractive optical elements embedded in dielectric waveguiding material as well as photonic crystal/bandgap structures. Non-homogeneous grid layouts are also possible as the local spatial resolution in each subspace can be varied, as long as the discrete time step is varied accordingly with respect to the stability criterion.

References

[1] K. S. Yee, "Numerical solution of initial boundary value problems involving Maxwells equations in isotropic media," *IEEE Trans. Antennas Propagat.*, vol. AP-14, pp. 302–307, Mar. 1966.

[2] A. Taflove, *Computational Electrodynamics: The Finite-Difference Time-Domain Method*. Boston, MA: Artech, 1995.

[3] ——, *Advances in Computational Electrodynamics: The Finite-Difference Time-Domain Method*. Boston, MA: Artech, 1998.

[4] R. W. Ziolkowski, "The incorporation of microscopic material models into the FDTD approach for ultrafast optical pulse simulations," *IEEE Trans. Antennas Propagat.*, vol. 45, pp. 375–391, Mar. 1997.

[5] K. H. Dridi and A. Bjarklev, "Optical electromagnetic vector-field modeling for the accurate analysis of finite diffractive structures of high complexity," *J. Appl. Optics*, vol. 38, no. 9, pp. 1668–1676, Mar. 1999.

[6] B. Gustafsson, H. O. Kreiss, and J. Oliger, *Time Dependent Problems and Difference Methods*: Wiley Interscience, 1995.

[7] K. W. Morton and D. E. Mayers, *Numerical Solution of Partial Differential Equations* Cambridge, 1994.

[8] K. H. Dridi, "Theoretical and numerical investigations of sub-wavelength diffractive optical structures," Ph.D. dissertation, Research Center COM, Technical Univ. Denmark, Lyngby, Denmark, Jan. 2000.
[9] T. Søndergaard and K. H. Dridi, "Energy flow in photonic crystal waveguides," *Physical Rev. B*, vol. 61, no. 23, pp. 15 688–15 696, June 15, 2000.
[10] B. Yang and J. S. Hesthaven, "A pseudospectral method for time-domain computation of electromagnetic scattering by bodies of revolution," *IEEE Trans. Antennas Propagat.*, vol. 47, pp. 132–141, Jan. 1999.
[11] B. Yang, D. Gottlieb, and J. S. Hesthaven, "Spectral simulations of electromagnetic wave scattering," *J. Comput. Phys.*, vol. 134, pp. 216–230, 1997.
[12] J. S. Hesthaven, P. G. Dinesen, and J. S. Lynov, "Spectral collocation time-domain modeling of diffractive optical elements," *J. Computational Phys.*, vol. 155, no. 2, pp. 287–306, Nov. 1, 1999.
[13] B. Yang and J. S. Hesthaven, "Multidomain pseudospectral computation of Maxwell's equations in 3-D general curvilinear coordinates," *Appl. Numerical Math.*, vol. 33, no. 1–4, pp. 281–289, May 2000.
[14] P. G. Dinesen, J. S. Hesthaven, J. P. Lynov, and L. Lading, "Pseudospectral method for the analysis of diffractive optical elements," *J. Opt. Soc. Amer. A*, vol. 16, no. 5, pp. 1124–1130, May 1999.
[15] J. S. Hesthaven, "Spectral penalty methods," *Appl. Numerical Math.*, vol. 33, pp. 23–41, 2000.
[16] A. C. Cangellaris and D. B. Wright, "Analysis of the numerical error caused by the stair-stepped approximation of a conducting boundary in FDTD simulations of electromagnetic phenomena," *IEEE Trans. Antennas Propagat.*, vol. 39, pp. 1518–1525, Oct. 1991.
[17] J. B. Schneider and K. L. Shlager, "FDTD simulations of TEM horns and the implications for staircased representations," *IEEE Trans. Antennas Propagat.*, vol. 45, pp. 1830–1838, Dec. 1997.
[18] S. Abarbanel, A. Ditkowski, and A. Yefet, "Bounded error schemes for the wave equation on complex domains," NASA Langley Research Center, Hampton, ICASE Report 9-50, Nov. 1998.
[19] S. Ramo, J. R. Whinnery, and T. Van Duzer, *Fields and Waves in Communication Electronics*, 3rd ed: Wiley, 1994.
[20] D. Gottlieb and B. Yang, "Comparisons of staggered and nonstaggered schemes for Maxwell's equations," in *Conf. Proc. 12th Annual Rev. Progress in Applied Computational Electromagnetics Naval Postgraduate School*, Monterey, CA, Mar. 18–22, 1996, p. 1122.
[21] B. Fornberg, "Calculation of weights in finite difference formulas," *SIAM Rev.*, vol. 40, pp. 685–691, Sept. 1998.
[22] C. Canuto, M. Y. Hussaini, A. Quarteroni, and T. A. Zang, *Spectral Methods in Fluid Dynamics*. New York: Springer-Verlag, 1988.
[23] A. Ditkowski, K. H. Dridi, and J. S. Hesthaven, Stable cartesian grid methods for Maxwell's equations in complex geometries. I. Second order schemes, 1999, to be published.

K. H. Dridi received the M.Sc. degree in electrical engineering from the Technical University of Denmark in 1997, with a curriculum including electronics, applied mathematics, electromagnetics and optics, and computer science. From 1997 to 2000 he conducted his Ph.D. studies at the research center for Communications, Optics, and Materials (COM) at the Technical University of Denmark

He is currently an Industrial Postdoc Fellow at ADC Telecommunications (Denmark), with an affiliation to the Optics and Fluid Dynamics Department at Risø National Laboratory. His research interests include subwavelength diffractive optical structures, photonic crystal waveguides, and computational methods, with applications to the telecommunications and information technology.

Jan S. Hesthaven received the M.Sc. and Ph.D degrees in applied mathematics/numerical analysis in 1991 and 1995, respectively, from the Technical University of Denmark.

He is currently an Assistant Professor of applied mathematics in the Division of Applied Mathematics, Brown University. His research interests include the accurate and efficient solution of wave-dominated problems in complex geometries, with contributions to finite-difference, spectral, and high-order finite element methods and with applications to problems in electromagnetics, gas-dynamics, acoustics, nonlinear optics and elasticity. For his research contributions he has been named a Sloan Research Fellow.

Adi Ditkowski received the B.Sc. degree in mathematics in 1990, the M.Sc. (*summa cum laude*) degree in applied mathematics in 1992, and the Ph.D degree in applied mathematics/numerical analysis in 1997, all from Tel-Aviv University.

He is currently a Visiting Assistant Professor in the Division of Applied Mathematics, Brown University. His research interests include developing finite-difference schemes for solving PDE's in complex geometries, analysis of errors in numerical schemes, and mathematical analysis and optimization of problems in materials science.